Author(s): Tomilov, A. & Videcoq, A. & Chartier, T. & Ala-Nissilä, Tapio & Vattulainen, I.

Title: Tracer diffusion in colloidal suspensions under dilute and crowded conditions with hydrodynamic interactions

Year: 2012

Version: Final published version

Please cite the original version:

Tomilov, A. & Videcoq, A. & Chartier, T. & Ala-Nissilä, Tapio & Vattulainen, I. 2012. Tracer diffusion in colloidal suspensions under dilute and crowded conditions with hydrodynamic interactions. The Journal of Chemical Physics. Volume 137, Issue 1. 014503. 0021-9606 (printed). DOI: 10.1063/1.4731661.

Tracer diffusion in colloidal suspensions under dilute and crowded conditions with hydrodynamic interactions

A. Tomilov, A. Videcoq, T. Chartier, T. Ala-Nissilä, and I. Vattulainen

Citation: The Journal of Chemical Physics **137**, 014503 (2012); doi: 10.1063/1.4731661
View online: http://dx.doi.org/10.1063/1.4731661
View Table of Contents: http://scitation.aip.org/content/aip/journal/jcp/137/1?ver=pdfcov
Published by the AIP Publishing

Tracer diffusion in colloidal suspensions under dilute and crowded conditions with hydrodynamic interactions

A. Tomilov,[1] A. Videcoq,[1,a)] T. Chartier,[1] T. Ala-Nissilä,[2,3] and I. Vattulainen[4,5]
[1]*SPCTS, UMR 7315, ENSCI, CNRS; Centre Européen de la Céramique, 12 rue Atlantis, 87068 Limoges cedex, France*
[2]*Department of Applied Physics and COMP CoE, Aalto University School of Science, P.O. Box 11100, FI-00076 Aalto, Espoo, Finland*
[3]*Department of Physics, Brown University, Providence, Rhode Island 02912-8143, USA*
[4]*Department of Physics, Tampere University of Technology, P.O. Box 692, FI-33101 Tampere, Finland*
[5]*MEMPHYS – Center for Biomembrane Physics, Department of Physics, Chemistry and Pharmacy, University of Southern Denmark, DK-5230 Odense, Denmark*

(Received 6 April 2012; accepted 13 June 2012; published online 3 July 2012)

We consider tracer diffusion in colloidal suspensions under solid loading conditions, where hydrodynamic interactions play an important role. To this end, we carry out computer simulations based on the hybrid stochastic rotation dynamics-molecular dynamics (SRD-MD) technique. Many details of the simulation method are discussed in detail. In particular, our choices for the SRD-MD parameters and for the different scales are adapted to simulating colloidal suspensions under realistic conditions. Our simulation data are compared with published theoretical, experimental and numerical results and compared to Brownian dynamics simulation data. We demonstrate that our SRD-MD simulations reproduce many features of the hydrodynamics in colloidal fluids under finite loading. In particular, finite-size effects and the diffusive behavior of colloids for a range of volume fractions of the suspension show that hydrodynamic interactions are correctly included within the SRD-MD technique. [http://dx.doi.org/10.1063/1.4731661]

I. INTRODUCTION

Understanding the behavior of colloidal suspensions is of great importance in various fields such as ceramic processing, coatings, paints, inks, drug delivery, and food processing. The applied field of ceramic processes is particularly exciting as the use of colloids in related applications is based on widely used and standardized processes. In order to develop new, improved and at the same time reliable processes, it is crucial that one has means to control the structural and rheological properties of the suspensions. Indeed, the colloidal arrangement in a suspension will largely determine both the suspension rheology that has to be rigorously controlled for the shaping process and the final material microstructure and material properties such as mechanical, optical, and electrical properties.

The conditions for reliability are particularly strict, highlighting the importance to have techniques that are able to accurately and reliably predict the behavior of a colloidal suspension. Numerical simulations comprising atomistic, molecular, and coarse-grained techniques are highly useful methods of choice to predict the properties of colloidal suspensions. However, being complex fluids, simulating the behavior of suspensions is not a simple feat. Colloids are characterized by sizes that range from a few nanometers to several micrometers, and their dynamics is characterized in a similar manner by a broad distribution of time scales up to seconds. Further, as there is a distinct separation of length and time scales between the dynamics of colloidal and solvent particles, the computational treatment of colloids under realistic hydrodynamic conditions is a daunting task. In practice, with the computational resources that are usually available the only appropriate way to consider colloidal dynamics is to coarse-grain the description of the solvent.

Perhaps the simplest technique developed for this purpose is Brownian dynamics (BD),[1] where Newton's equations of motion (in terms of the Langevin equation) are solved for each colloid, including the effect of fluid on the colloids in terms of dissipative and random thermal forces. Because of its simplicity, this technique is widely used and has quite often been able to make appropriate predictions concerning the behavior of suspensions, e.g., in heteroaggregation (suspension stability, aggregate structure, aggregation kinetics, porosity, and percolation threshold).[2–5] Nevertheless, BD neglects the many-body hydrodynamic interactions (HIs) (i.e., momentum transport through the fluid) that are known to play an important role especially in concentrated colloidal suspensions.

Consequently, several other simulation techniques have emerged in order to take the HIs into account. Stokesian dynamics[6] uses higher-order terms in a multipole expansion of hydrodynamic interactions, so it is an improvement compared to BD, but the downside is that it is relatively slow. The Lattice-Boltzmann (LB) method, which is an efficient way to solve for the Navier-Stokes equations of hydrodynamics has been extended to include colloidal particles;[7,8] however, artificial Langevin noise has to be added to the colloidal particles to achieve thermal equilibrium.[9,10] Recently, a new fluctuating LB method has been presented, where this

a)Author to whom correspondence should be addressed. E-mail: arnaud.videcoq@unilim.fr.

problem has been solved,[11] making the method the first quantitatively predictive multi-scale simulation method of its kind at present. Another coarse-grained method that naturally incorporates thermal fluctuations, namely dissipative particle dynamics (DPD) (Refs. 12, 13) has become standard molecular dynamics (MD) technique that is based on specifically chosen dissipative and thermal forces that are bridged to one another in a manner which conserves local momentum. While it is an appropriate method for many situations, its main challenge in terms of computational effort is to deal with systems with a large number of solvent particles, since they are explicitly treated.

The technique that we will adopt in the present case is the stochastic rotation dynamics (SRD) method (also called multi-particle collision dynamics) derived by Malevanets and Kapral.[14] In SRD, space is partitioned into cubic cells, and at discrete time intervals the coarse-grained fluid particles inside each cell exchange momentum by rotating their velocities relative to the center of mass velocity of all the particles in the given cell. SRD is particularly adapted to the simulation of mesoscopic particles embedded in a fluid. Malevanets and Kapral derived a hybrid SRD-MD algorithm that combines a full MD scheme for the colloid-colloid and colloid-fluid interactions, with a treatment of the fluid-fluid interactions via SRD.[15] SRD-MD has been found to be a good compromise between good precision of results and relatively low computational cost.[16] Nevertheless, even though SRD-MD has already been used to simulate colloidal suspensions,[17–21] its use remains quite tricky and several different implementations have been developed.

In this paper, we use the hybrid SRD-MD technique to simulate a realistic model of a colloidal, aqueous suspension based on spherical silica particles of diameter ≈600 nm. Such a ceramic system has been previously studied both experimentally and by means of BD simulations, when two populations of colloids with different surface properties were present.[4,5] Here, we consider identical colloids, with a unimodal size distribution interacting through soft repulsive potentials, and we study the colloids' tracer diffusion coefficient $D_T(\phi_c)$ as a function of the colloidal volume fraction ϕ_c. This constitutes a good model system in order to test if our 3D SRD-MD simulations correctly describe the hydrodynamics in the system, since hydrodynamic interactions play an increasing role when the colloid volume fraction increases.[22] Second, after validation of the model, its implementation provides an opportunity to make predictions for the complex dynamics of colloids under both dilute and crowded conditions.

This paper is organized as follows. Section II summarizes the description of our simulation methodology. The SRD-MD technique used in this paper is first described, along with our choice of the SRD parameters and interaction potentials. Then, we explain how the various physical scales have been chosen in order to map the coarse-grained simulation to our real colloidal system. As we are interested in the dynamical properties of this system, we describe how the solvent viscosity and the tracer diffusion coefficient of both fluid and colloidal particles are computed in the simulations. The results are presented and discussed in Sec. III. On the basis of the fluid properties, we first explain our choice of the fluid particle number as a function of the colloidal volume fraction. Effects of finite system size are also discussed. Then, results concerning the colloidal tracer diffusion coefficient as a function of the colloid volume fraction are presented. In particular, we discuss the nature of short and long-time diffusive behavior using the SRD-MD method. The results are also compared with new BD simulation data using the same interaction potentials as for the SRD-MD case.

II. SIMULATION METHODOLOGY

A. Pure fluid (SRD)

The fluid is represented by N_f point-like particles, each having a mass m_f. Their dynamics consists in a succession of streaming steps of duration Δt_{SRD} interrupted by multi-particle collisions, in which the fluid particles exchange momentum. During streaming steps, the position of particle i, $\mathbf{x}_i$, is updated as follows:

$$\mathbf{x}_i(t + \Delta t_{SRD}) = \mathbf{x}_i(t) + \mathbf{v}_i(t)\Delta t_{SRD}, \tag{1}$$

where $\mathbf{v}_i$ denotes the velocity of the particle. For collision steps, space is partitioned into cubic cells (collision volumes) of linear size a_0, and during a collision event the velocity of each fluid particle relative to the center of mass velocity of all the particles in the given cell is rotated by an angle α around an axis chosen randomly for each cell:

$$\mathbf{v}_i(t + \Delta t_{SRD}) = \mathbf{v}_{cm} + \mathbf{R}(\mathbf{v}_i(t) - \mathbf{v}_{cm}), \tag{2}$$

where $\mathbf{v}_{cm}$ is the center of mass velocity of all the particles in the cell the particle i belongs to, and $\mathbf{R}$ is the rotation matrix. This procedure conserves energy and momentum locally and thus provides the correct hydrodynamics as described by the continuum Navier-Stokes equations.

In an SRD simulation, lengths are expressed in units of the linear size of collision cells a_0, energies in units of k_BT and masses in units of the fluid particle mass m_f. Time is expressed in units of $t_0 = a_0\sqrt{m_f/k_BT}$. The fluid properties (such as viscosity and the Schmidt number S_c) depend on the three following independent SRD parameters:

- The dimensionless mean free path

$$\lambda = \frac{\Delta t_{SRD}}{t_0}, \tag{3}$$

  which provides a measure of the average fraction of cell size that a fluid particle travels between collisions. For the simulation of a liquid rather than a gas, it is important to keep the value of $\lambda \ll 1$. However, decreasing λ increases the simulation time.
- The average number of fluid particles per collision cell γ that does not strongly influence fluid properties. It is advisable to keep the value of γ relatively small ($\leq$10) in order to maintain reasonable computational efficiency.
- The rotation angle α, for which high values lead to high Schmidt numbers. Because of this values in the range of [90° ; 170°] should be used.

The relative simplicity of the fluid particle dynamics in SRD has allowed the derivation of analytic expressions for

the fluid properties as functions of the three SRD parameters (λ, γ, and α).[23,24] The normalized diffusion coefficient of a fluid particle is given by

$$\frac{D_f}{D_0} = \lambda\left[\frac{3}{2[1-\cos(\alpha)]}\left(\frac{\gamma}{\gamma-1}\right)-\frac{1}{2}\right]. \quad (4)$$

The kinematic viscosity of the fluid is the sum of a kinetic contribution that dominates for a gas and a collisional contribution, which is dominant for a liquid, $\nu = \nu_{kin} + \nu_{col}$, and the two contributions are given by

$$\frac{\nu_{kin}}{\nu_0} = \frac{\lambda}{3}\left[\frac{15\gamma}{(\gamma-1+e^{-\gamma})[4-2\cos(\alpha)]-2\cos(2\alpha)}-\frac{3}{2}\right], \quad (5)$$

$$\frac{\nu_{col}}{\nu_0} = \frac{1}{18\lambda}[1-\cos(\alpha)](1-1/\gamma+e^{-\gamma}/\gamma). \quad (6)$$

The units of particle self diffusion and kinematic viscosity are $D_0 = \nu_0 = a_0^2/t_0$, and the ratio of momentum diffusivity to mass diffusivity gives the Schmidt number as $S_c = \nu/D_f$.

As proposed by Padding and Louis[16] for the simulation of a colloidal suspension, we have chosen the three SRD parameters to be as follows: $\lambda = 0.1$, $\gamma = 5$, and $\alpha = \pi/2$. These parameter values give a Schmidt number of the order of three. Even if this value is low compared to the Schmidt number of a real solvent (water), the authors claim that this should be enough to reproduce correctly the hydrodynamics of the system. This has also been earlier verified in the SRD-MD simulations of Falck *et al.* for dense 2D colloidal systems.[17]

It is worth noticing that when the average distance that a fluid particle travels between collisions is small compared to the linear size of the cells ($\lambda \ll 1$), the fluid particles remain in the same cell for several time steps and there are correlations between the collision events that break Galilean invariance. One way to solve this problem has been proposed by Ihle and Kroll.[25] It consists of a translation of all fluid particles by a vector, whose coordinates are randomly chosen in the range $[-a_0/2; a_0/2]$, to be carried out just before the collision. After the collision event, the fluid particles are moved back to their previous positions. This grid shifting procedure has been applied in the present SRD simulations.

B. Colloids embedded in the fluid (hybrid SRD-MD)

1. Basic principles

Colloids are treated microscopically by MD, with microscopically defined colloid-colloid and colloid-fluid interactions. The colloid-fluid interactions are also included into the streaming steps of SRD. Hence, fluid and colloidal particles obey Newton's laws of motion:

$$\frac{d\mathbf{x}_i}{dt} = \mathbf{v}_i \quad \text{and} \quad m_i\frac{d\mathbf{v}_i}{dt} = \mathbf{F}_i, \quad (7)$$

where $\mathbf{F}_i$ is the external force applied to particle i.

For fluid particles, the only contribution to this force comes from moving boundary conditions constituted by the surface of the colloids. In the present simulations this force is assumed to come from a radial colloid-fluid interaction potential V_{cf}. The interaction potential between fluid particles is assumed to be zero ($V_{ff} = 0$). The exchange of momentum between fluid particles takes place in the collision events of SRD. On the other hand, the force applied to the colloids contains two contributions: one coming from fluid particles (interaction potential V_{cf}) and one coming from the other colloids (interaction potential V_{cc}). With all these interaction potentials defined, Eqs. (7) are solved using the velocity-Verlet algorithm, with a time step Δt_{MD} shorter than Δt_{SRD}.

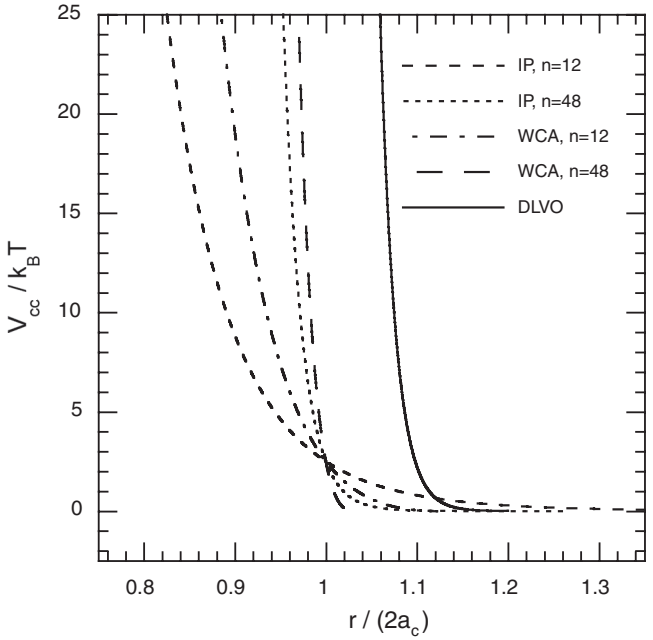

FIG. 1. Colloid-colloid interaction potentials as a function of the dimensionless center-to-center separation distance (see text for details).

2. Interaction potentials

a. Colloid-colloid interaction. For describing the colloid-colloid interaction, we have employed inverse-power (IP) pair potentials that are commonly used for hard-sphere colloids (see for examples the 2D studies of Refs. 17, 26):

$$V_{cc}(r) = \begin{cases} \varepsilon_{cc}\left(\frac{\sigma_{cc}}{r}\right)^n & (r \le r_c); \\ 0 & (r > r_c), \end{cases} \quad (8)$$

where r is the center-to-center separation distance. We used two values for n, namely $n = 12$ with $r_c \equiv 2.5\sigma_{cc}$, and $n = 48$ with $r_c \equiv 1.26\sigma_{cc}$. We define an effective radius for the colloids through the interaction parameter σ_{cc} as $a_c = \sigma_{cc}/2$, and $\varepsilon_{cc} = 2.5k_BT$. These two potentials are plotted in Fig. 1.

For comparison, we have also plotted in Fig. 1 the Weeks-Chandler-Andersen (WCA) potential:

$$V_{cc}(r) = \begin{cases} 4\varepsilon_{cc}\left[\left(\frac{\sigma_{cc}}{r}\right)^n - \left(\frac{\sigma_{cc}}{r}\right)^{n/2} + \frac{1}{4}\right] & (r \le r_c \equiv 2^{2/n}\sigma_{cc}), \\ 0 & (r > r_c), \end{cases} \quad (9)$$

with $n = 12$ and $n = 48$. The WCA potential has been used for example in a previous study concerning the SRD-MD technique[16] and in a study of 3D colloidal diffusion with the DPD technique.[27]

In Fig. 1, we also depict the Derjaguin Landau Verwey Overbeek (DLVO) potential that we have used in our previous studies of ceramic suspensions to describe the interaction between charged silica particles.[4] This potential is the sum of two contributions: attraction due to van der Waals forces V_{cc}^{vdW} and electrostatic double layer interaction V_{cc}^{el} due to the surface charges of the colloids:

$$V_{cc}^{DLVO} = V_{cc}^{vdW} + V_{cc}^{el}. \tag{10}$$

The van der Waals contribution is[28]

$$V_{cc}^{vdW}(r) = -\frac{A}{6}\left[\frac{2a_c^2}{r^2-4a_c^2} + \frac{2a_c^2}{r^2} + \ln\left(\frac{r^2-4a_c^2}{r^2}\right)\right], \tag{11}$$

where $A = 4.6 \times 10^{-21}$ J is the Hamaker constant for silica in water.[29,30] The electrostatic term (interaction at constant surface potentials)[31] is given by

$$V_{cc}^{el}(r) = \pi\varepsilon a_c \psi^2 \left[\ln\left(\frac{1+e^{-\kappa h}}{1-e^{-\kappa h}}\right) + \ln\left(1-e^{-2\kappa h}\right)\right], \tag{12}$$

where $\varepsilon = \varepsilon_0\varepsilon_r$ is the dielectric constant of the solvent ($\varepsilon_r = 81$ for water), ψ is the surface potential of the particle, $h = r - 2a_c$ is the surface-to-surface separation distance, and κ is the inverse Debye screening length. The surface potential and the inverse Debye screening length are deduced from experimental measurements: the value of the zeta potential is used for the surface potential ($\psi = -52$ mV, measured at pH = 5.5) and the value $\kappa = 10^8$ m^{-1} comes from conductivity measurements.[4]

In these conditions of pH and ionic strength, the DLVO potential exhibits a strong, short-range repulsion that prevents from the particle aggregation, in accordance with sedimentation tests, which have experimentally proven the suspension stability.[4] Thus, our aim is here to describe a system with no aggregation and we note that the DLVO potential, with the parameters used here, has a shape very close to the purely repulsive IP potential of Eq. (8), with $n = 48$, so that results provided by those potentials should be very similar under a rescaling of the colloid size.

b. Colloid-fluid interaction. The coupling between the dynamics of colloids solved by MD and the fluid solved by SRD is treated by radial interactions between the colloid and fluid particles that intervene into the MD steps. The potential used here for this repulsion is an IP potential:

$$V_{cf}(r) = \begin{cases} \varepsilon_{cf}\left(\frac{\sigma_{cf}}{r}\right)^n & (r \le r_c \equiv 2.5\sigma_{cf}), \\ 0 & (r > r_c), \end{cases} \tag{13}$$

with $n = 12$.

As suggested by Padding and Louis,[16] the colloid-fluid interaction parameter σ_{cf} has been taken to be smaller than the colloid radius ($\sigma_{cf} < a_c$). This lets the fluid particles penetrate in between two colloids, so that spurious depletion attraction between colloids is avoided. This also mimics lubrication forces between the colloids. A value of $\sigma_{cf} = 0.8a_c$ is used here, and $\varepsilon_{cf} = \varepsilon_{cc} = 2.5k_BT$.

A WCA potential could also be used for the colloid-fluid repulsion,[16]

$$V_{cf}(r) = \begin{cases} 4\varepsilon_{cf}\left[\left(\frac{\sigma_{cf}}{r}\right)^n - \left(\frac{\sigma_{cf}}{r}\right)^{n/2} + \frac{1}{4}\right] & (r \le r_c \equiv 2^{2/n}\sigma_{cf}); \\ 0 & (r > r_c), \end{cases} \tag{14}$$

with $n = 12$. For this potential we have found out that a value of $\sigma_{cf} = 0.9a_c$ is sufficient to avoid depletion attraction between colloids.

According to this choice of the potentials, we have used the following MD time step: $\Delta t_{MD} = \Delta t_{SRD}/8$. This value has been adjusted in order to conserve energy in the simulation (at constant temperature).

C. Length, mass, and time scales

Our aim is to simulate the behavior of a realistic colloidal suspension. In order to choose the various scales, we have applied the mapping between the physical and coarse-grained systems as described in Ref. 16.

1. Length scale

The linear size of the collision cells is fixed to half the colloid radius:

$$a_0 = \frac{a_c}{2} = 1.5 \times 10^{-7}\text{m}. \tag{15}$$

This value should give a good compromise between resolution and computational cost.[16]

2. Mass scale

The mass of the fluid particle m_f is fixed in order to obtain the correct physical value for the fluid mass density $\rho_f = 1000$ kg m^{-3} (as for water):

$$m_f = \frac{a_0^3\rho_f}{\gamma} = 6.75 \times 10^{-19}\text{kg}. \tag{16}$$

The mass of a colloid corresponds to the mass of a silica sphere of radius a_c:

$$M_c = \frac{4}{3}\pi a_c^3\rho_c = 2.49 \times 10^{-16}\text{kg} \approx 369m_f, \tag{17}$$

with the silica mass density of $\rho_c = 2200$ kg m^{-3}.

3. Time scale

As SRD-MD is compacting the large physical hierarchy of time scales, it is not possible to correctly reproduce all the relevant time scales. Here, we have chosen to map the larger time scales, i.e., the diffusion time,

$$\tau_D = \frac{a_c^2}{D_0}, \tag{18}$$

which is the time for a colloid to diffuse over its radius and where D_0 is the (tracer) diffusion coefficient of a colloid. In

order to evaluate τ_D, we use the standard Stokes-Einstein expression of the colloid diffusion coefficient

$$D_0 = \frac{k_B T}{\zeta}, \tag{19}$$

where ζ is the hydrodynamic friction coefficient $\zeta = 6\pi\eta a_c$, for the stick boundary conditions at the colloid surface, and η is the shear viscosity of the solvent. Using $T = 293$ K and $\eta = 10^{-3}$ Pa s (for water), the evaluation of the real physical values of the diffusion coefficient and of the diffusion time gives $D_0 = 7.15 \times 10^{-13}$ m^2 s^{-1} and $\tau_D = 0.126$ s, respectively.

In the present simulations, as we have radial interactions between colloids and fluid particles, which do not transfer angular momentum to a spherical colloid, effective slip boundary conditions are induced. We can evaluate the friction coefficient generated by the simulated liquid. There are two sources of friction.[16] The first comes from the local Brownian collisions with the small particles and can be calculated by a simplified Enskog-Boltzmann-type kinetic theory adapted here for slip boundary conditions:

$$\zeta_E = \frac{8}{3}\left(\frac{2\pi k_B T M_c m_f}{M_c + m_f}\right)^{1/2} n_f \sigma_{cf}^2 = \frac{8}{3}\left(2\pi\frac{M_c}{M_c + m_f}\right)^{1/2} \gamma \left(\frac{\sigma_{cf}}{a_0}\right)^2 \frac{m_f}{t_0} = \xi_E \frac{m_f}{t_0}, \tag{20}$$

where $n_f = \gamma/a_0^3$ is the fluid particle number density. The second contribution is the Stokes friction, ζ_S, for which a substantial system-size effect is expected, since it depends on long-range hydrodynamic effects. These can be expressed in terms of a correction factor $f(\sigma_{cf}/L)$:

$$\zeta_S = \frac{4\pi\eta\sigma_{cf}}{f(\sigma_{cf}/L)}. \tag{21}$$

The correction factor should scale as

$$f(\sigma_{cf}/L) \approx 1 - 2.837\frac{\sigma_{cf}}{L}. \tag{22}$$

If we do not take this correction into account and use $\eta = \nu\rho_f = \nu\gamma m_f/a_0^3$, we find

$$\zeta_S = 4\pi\left(\frac{\nu_{kin}}{\nu_0} + \frac{\nu_{col}}{\nu_0}\right)\gamma\frac{\sigma_{cf}}{a_0}\frac{m_f}{t_0} = \xi_S\frac{m_f}{t_0}. \tag{23}$$

These two contributions to the friction should be added in parallel to obtain the total friction,

$$\frac{1}{\zeta} = \frac{1}{\zeta_S} + \frac{1}{\zeta_E}, \tag{24}$$

such that

$$\zeta = \left(\frac{1}{\xi_S} + \frac{1}{\xi_E}\right)^{-1}\frac{m_f}{t_0} = \xi\frac{m_f}{t_0}. \tag{25}$$

Thus, the colloid diffusion coefficient is given by

$$D_0 = \frac{k_B T}{\zeta} = \frac{1}{\xi}\frac{a_0^2}{t_0} \tag{26}$$

and the diffusion time is

$$\tau_D = \frac{a_c^2}{D_0} \simeq \frac{\sigma_{cf}^2}{D_0} = \xi\left(\frac{\sigma_{cf}}{a_0}\right)^2 t_0. \tag{27}$$

Equating this time to the real physical value of the diffusion time fixes the time scale as $t_0 = 7.37 \times 10^{-4}$ s.

4. Temperature scale

When the length, mass, and time scales are fixed, the temperature scale is also fixed as

$$T = \frac{a_0^2 m_f}{k_B t_0^2} = 2.02 \times 10^{-3}\text{K}. \tag{28}$$

D. Calculation of dynamical properties

As we are interested in the dynamical properties of the colloidal system, we compute in the simulations the viscosity associated to the fluid particles and the tracer diffusion coefficients of both the fluid and colloidal particles.

1. Fluid viscosity

The shear viscosity of the fluid is calculated from the stress autocorrelation function[15,25,32]

$$\eta = \frac{m_f^2 n_f \Delta t_{SRD}}{N_f k_B T}\left(\frac{1}{2}\left\langle\sigma_{xy}^2(0)\right\rangle + \sum_{k=1}^{\infty}\langle\sigma_{xy}(t)\sigma_{xy}(0)\rangle\right), \tag{29}$$

where $t = k\Delta t_{SRD}$ and

$$\sigma_{xy}(t) = -\frac{1}{\Delta t_{SRD}}\sum_{i=1}^{N_f}\left[v_{ix}(t)\Delta\xi_{iy}(t) + \Delta v_{ix}(t)\Delta\xi_{iy}^S(t)\right], \tag{30}$$

with $\Delta\xi_{iy}(t) = \xi_{iy}(t + \Delta t_{SRD}) - \xi_{iy}(t)$, $\Delta\xi_{iy}^S(t) = \xi_{iy}(t + \Delta t_{SRD}) - \xi_{iy}^S(t + \Delta t_{SRD})$, and $\Delta v_{ix}(t) = v_{ix}(t + \Delta t_{SRD}) - v_{ix}(t)$. The quantity $\xi_i(t)$ is the cell coordinate of particle i at time t and $\xi_i^S(t)$ is its cell coordinate in the shifted frame (using the grid shifting procedure). The ratio $n_f = N_f/V_f$ is the fluid number density, where V_f denotes the volume that can be occupied by the fluid particles.

2. Tracer diffusion coefficient

The tracer diffusion coefficient of either fluid particles or colloids can be computed in the following three different ways:[16,17,33]

a. Velocity autocorrelation function. The time integral of the velocity autocorrelation function: $\varphi(t) \equiv \langle\mathbf{v}_i(t)\cdot\mathbf{v}_i(0)\rangle$, where $\mathbf{v}_i(t)$ is the velocity of particle i at time t, gives the time-dependent transport coefficient as

$$D_T(t) = \frac{1}{dN}\sum_{i=1}^{N}\int_0^t \mathrm{d}t'\langle\mathbf{v}_i(t')\cdot\mathbf{v}_i(0)\rangle. \tag{31}$$

The average is taken over all the N identical particles and $d = 3$ is the dimensionality of the system. The tracer diffusion coefficient corresponds to the hydrodynamic limit $D_T = \lim_{t\to\infty} D_T(t)$.

b. Displacement autocorrelation function. The displacement autocorrelation function is $C_T(t) \equiv \langle\delta\mathbf{r}_i(t)\cdot\delta\mathbf{r}_i(0)\rangle$,

where $\delta\mathbf{r}_i(t_m)$ is the change in the position of particle i in between two consecutive discrete time steps: $t_m = m\tau_0$ and $t_{m-1} = (m-1)\tau_0$. The tracer diffusion coefficient is then given by

$$D_T = \frac{1}{d\tau_0 N}\sum_{i=1}^{N}\left[\frac{1}{2}\langle\delta\mathbf{r}_i(0)\cdot\delta\mathbf{r}_i(0)\rangle + \sum_{k=1}^{\infty}\langle\delta\mathbf{r}_i(k\tau_0)\cdot\delta\mathbf{r}_i(0)\rangle\right]. \tag{32}$$

c. Mean-square displacement. The tracer diffusion coefficient can also be computed from the mean-square displacement

$$D_T = \lim_{t\to\infty}\frac{1}{2dNt}\sum_{i=1}^{N}\langle[\mathbf{r}_i(t)-\mathbf{r}_i(0)]^2\rangle. \tag{33}$$

III. RESULTS AND DISCUSSION

Most of the simulations were performed in a cubic box whose linear size is $L = 32a_0$, after considering the finite-size effects (cf. Sec. III B). The number of colloidal particles N_c was varied and the relevant parameter that we use is the effective colloidal volume fraction, i.e., the ratio between the volume occupied by the colloids and the total volume of the simulation box, defined as

$$\phi_c = \frac{\frac{4}{3}\pi a_c^3 N_c}{(32a_0)^3}. \tag{34}$$

We note that the value of the particle radius a_c is not uniquely defined for particles, which interact through IP potentials as in the present case. Further, the hydrodynamic radius of the particles is not well-defined in the SRD-MD method, either.[11] Thus, the above definition of ϕ_c should be considered as an effective volume fraction, which should be rescaled appropriately to facilitate comparison with hard-core particles. We will discuss this issue further in Sec. III D.

The initial configurations were generated as follows. For $\phi_c \le 0.3$, colloids are initially placed at random, non-overlapping positions in the simulation box, while above this volume fraction they are placed at regular lattice positions. The fluid particles are always placed at random positions, but at a distance larger than σ_{cf} of the center of any colloid. Initial random velocities with a Maxwell distribution are attributed to all particles. Then, the system is equilibrated (possibly at higher temperature for high volume fractions, in order to minimize the influence of the initial lattice positions). At the beginning of these steps the relaxation of the system makes the potential energy decrease and, consequently, because of total energy conservation, the kinetic energy increases. A rescaling of all velocities is therefore also performed during the equilibration steps. The real simulation starts afterward, and the quantities needed for the computation of dynamical properties are stored.

A. Number of fluid particles

In a simulation without any colloids, the number of fluid particles is $N_f = 32^3\gamma = 163\,840$. As the coupling between the MD of the colloids and the SRD of the fluid particles is realized by colloid-fluid interactions, the fluid particles can only slightly penetrate the surface of the colloids. As a consequence, it seems logical to decrease the number of fluid particles as ϕ_c is increased, taking into account that the free volume for the fluid particles is actually $V_f = (32a_0)^3 - N_c\frac{4}{3}\pi\sigma_{cf}^3$, which decreases as N_c increases. Nevertheless, we tried both cases (a decreasing number of fluid particles and a constant one) and calculated the dynamical properties associated to the fluid particles (viscosity with Eq. (29), the self-diffusion coefficient with Eq. (32), and the Schmidt number) as a function of the colloidal volume fraction. The Schmidt number is shown in Fig. 2.

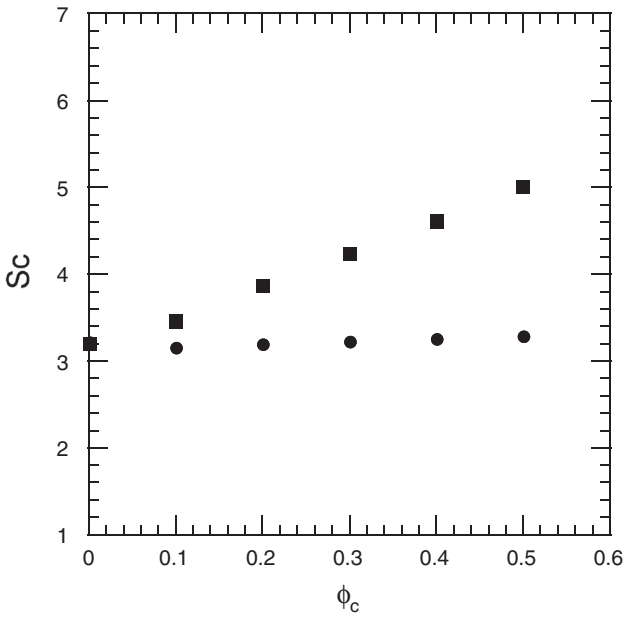

FIG. 2. Schmidt number as a function of the colloidal volume fraction in the case where the number of fluid particles is decreased (disks) and when it is kept constant (squares).

It can be seen that S_c only weakly depends on the volume fraction when the number of fluid particles remains constant. However, when fluid particles are removed with increasing ϕ_c there is no change in S_c, and thus we have chosen this option in the simulations. We have additionally checked that keeping N_f constant has virtually no influence on the results shown in Secs. III B–III D. Table I summarizes the values of N_c and N_f used for different colloid volume fractions.

In the following, we concentrate on the colloidal tracer diffusion coefficient computed by Eqs. (31)–(33). Averages are taken over the different colloids and time steps. For each simulation run, the number of SRD time steps was chosen

TABLE I. Number of colloids and fluid particles as a function of the colloidal volume fraction. The numbers are used within a simulation box of 32 × 32 × 32 collision cells and with the colloid-fluid interaction potential given by Eq. (13).

ϕ_c	0.001	0.1	0.2	0.3	0.4	0.5	0.6
N_c	1	98	196	293	391	489	587
N_f	163754	155433	147026	138705	130298	121890	113483

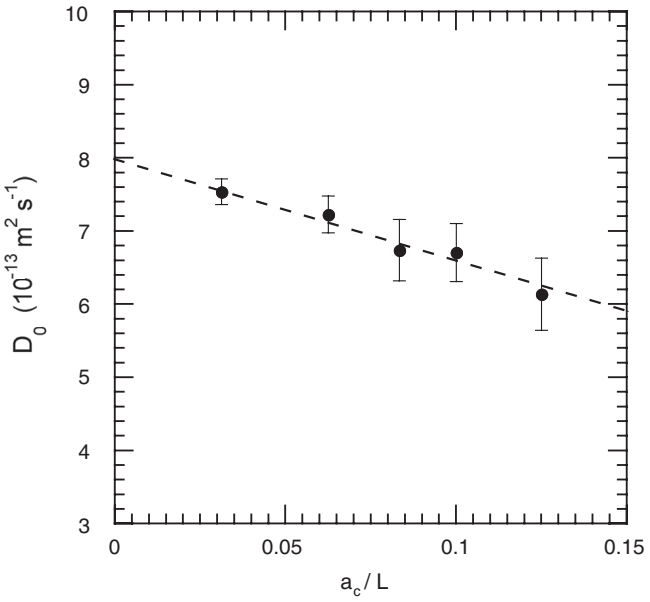

FIG. 3. Colloidal tracer diffusion coefficient under high dilution D_0 as a function of a_c/L ($a_c = 2a_0$). The results compare well to the dashed line that is a linear fit with the slope given by Eq. (36).

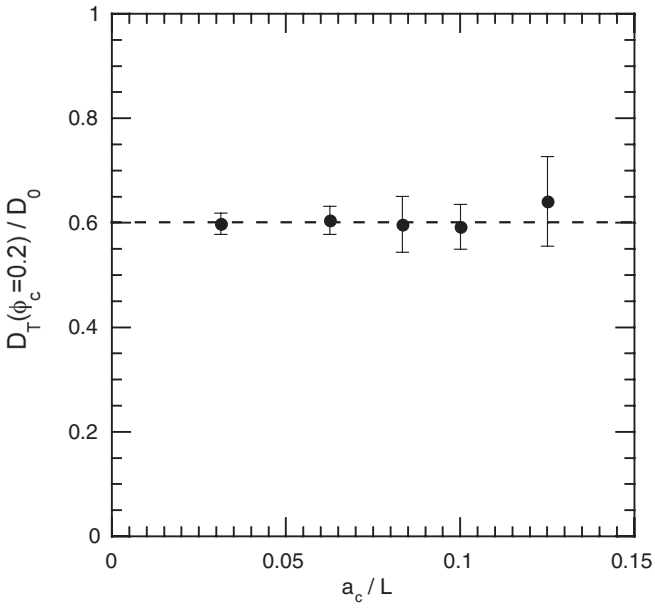

FIG. 4. Dimensionless colloidal tracer diffusion coefficient for a colloid volume fraction equal to 0.2 as a function of a_c/L. The dashed line that corresponds to a constant value is a guide to the eye.

so that the product $N_c \times N_{\text{SRD time steps}}$ is at least equal to, namely 10^6 for $\phi_c = 0.001$, 5×10^6 for $0.008 \leq \phi_c \leq 0.2$ and 10^7 for $\phi_c > 0.2$. The average values and error bars are computed from at least three separate simulation runs in each case.

B. Finite size effects

In any numerical simulation with HIs, it is imperative to take into account the finite-size effects because of the long-range nature of the HIs. Let us first consider the highly diluted case. Simulations were performed for different box sizes, namely $L = 16a_0$, $20a_0$, $24a_0$, $32a_0$, and $64a_0$, with a constant colloidal volume fraction $\phi_c \approx 0.008$, which corresponds to one colloid in the smallest box, and the colloidal tracer diffusion coefficient $D_T \approx D_0$ was computed. Results are shown in Fig. 3.

As discussed in Sec. II C 3, the tracer diffusion coefficient for a single colloid D_0 can be expressed as

$$D_0 = \frac{k_B T}{\zeta} = k_B T \left(\frac{1}{\zeta_S} + \frac{1}{\zeta_E} \right), \tag{35}$$

with the box size dependence of the Stokes friction given by Eqs. (21) and (22), because of the HIs. Consequently, D_0 should behave as

$$D_0 = \frac{k_B T}{\zeta} = k_B T \left(\frac{1}{4\pi\eta\sigma_{cf}} + \frac{1}{\zeta_E} \right) - 2.837 \frac{k_B T}{4\pi\eta a_c} \frac{a_c}{L}. \tag{36}$$

As shown in Fig. 3, the slope $-2.837 k_B T/(4\pi\eta a_c)$ provides a very good fit to the system size dependence, telling us that the long-range hydrodynamic effects are well reproduced in the present simulations. For the shear viscosity, we have used here the value given by Eqs. (5) and (6): $\eta = 1.52 \times 10^{-8}$ Pa s, which is in agreement with the value computed in the simulations using Eq. (29). To check the consistency of the finite-size dependence for finite volume fractions, in Fig. 4 we show the normalized (dimensionless) tracer diffusion coefficient $D_T(\phi_c = 0.2)/D_0$. These data show that when normalized with D_0, the volume fraction dependent tracer diffusion coefficients should be independent of the system size within the statistical accuracy of the data. We note that the same conclusion was also drawn for the 2D case in Ref. 17.

C. Short and long time diffusion

To study the volume fraction dependence of colloidal dynamics we performed extensive simulations for a wide range of values of ϕ_c, from the dilute case ($\phi_c = 0.001$ corresponding to a single particle for $L = 32$) up to a highly concentrated suspension with $\phi_c = 0.6$. All data shown here are for the case of an inverse power law colloid-colloid interaction potential given by Eq. (8), with either $n = 12$ or $n = 48$. For each case, the colloid tracer diffusion coefficient has been computed using Eqs. (31)–(33). We first note that results from the velocity autocorrelation function and from the displacement autocorrelation function (Eqs. (31) and (32)) give exactly the same results, which is a good consistency check for diffusion.

To begin with, from the simulation with only one colloid, which corresponds to the volume fraction of 0.001, one can deduce the colloid tracer diffusion coefficient in infinite dilution. We find out the value $D_0 = (7.2 \pm 0.2) \times 10^{-13}$ m^2 s^{-1}, which is in very good agreement with the theoretical value of the diffusion coefficient given by Eq. (19) ($D_0 = 7.15 \times 10^{-13}$ m^2 s^{-1}). This means that the methodology explained in Ref. 16 and employed in Sec. II C 3 to derive the time scale works well.

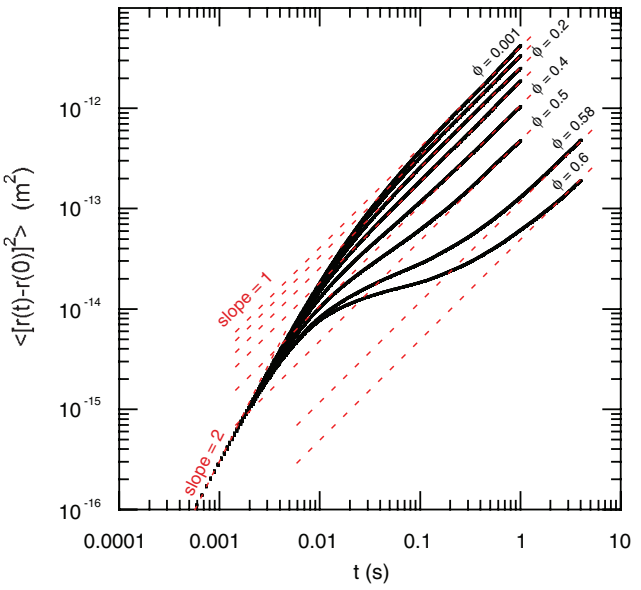

FIG. 5. Log-log plot of the colloid mean-squared displacement for colloid volume fractions of 0.001, 0.1, 0.2, 0.3, 0.4, 0.5, 0.58, and 0.6. Here, the power of the IP colloid-colloid potential is $n = 12$.

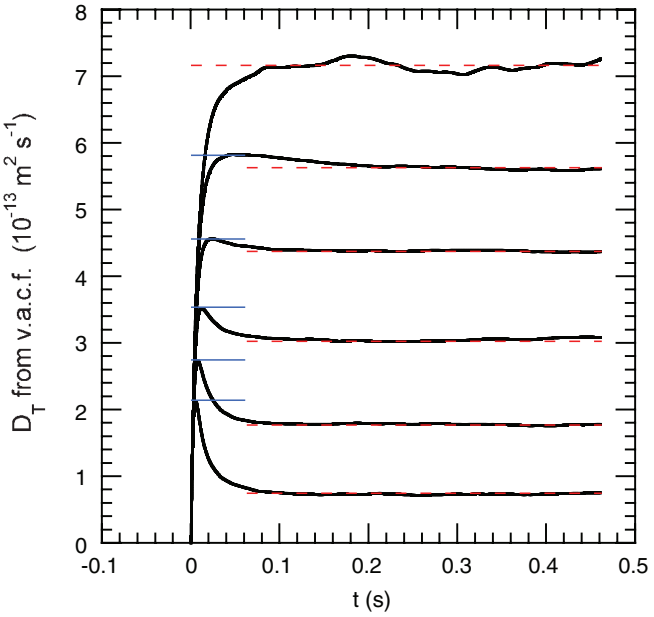

FIG. 6. $D_T(t)$ computed from the velocity autocorrelation function. From top to bottom the colloidal volume fraction is equal to 0.001, 0.1, 0.2, 0.3, 0.4, and 0.5. The red dashed lines correspond to the value of D_T as obtained from the mean-square displacement. The blue lines at short times indicate the value of $\tilde{D}_T^S(\phi_c)$ (see text for details).

Next, we discuss the mean-square displacements (MSD) of the colloidal particles. In Fig. 5, we show data for the case where the exponent $n = 12$ for the IP colloid-colloid potential.

From the data it can be clearly seen that at very early times the MSD follows a power law behavior in time with an exponent of two, which characterizes pre-diffusive, ballistic behavior.[27,34,35] For hard particles it is also theoretically expected[36] that for finite concentrations there is also a well-defined short-time diffusion coefficient D_T^S, which is associated with the time scale separation between local, short-time motion of the colloidal particles and the asymptotic Brownian behavior. The physical explanation for dense systems is that there is a finite amount of free space (unoccupied by other colloids) around each colloid and thus the mobility of the colloids within a short distance (fraction of the colloid radius) is faster than the asymptotic diffusion over a larger distance, which involves the coordinated displacement of several colloids. Hydrodynamic effects are essentially included in the short-time tracer diffusion coefficient, while the direct interactions are dominant at long times. Medina-Noyola[37] has suggested as a first approximation for self-diffusion at high volume fractions, to decouple the hydrodynamic effects from the direct interactions as

$$D_T/D_0 = D_T^S/D_0 \cdot D_T^H/D_0, \tag{37}$$

where D_T^H is the asymptotic (long-time) self-diffusion coefficient in the absence of hydrodynamic interactions. However, as can be seen in Fig. 5, in the present case there seems to be no well-defined D_T^S, as the MSD curves do not show a clear intermediate linear regime before crossing over to the asymptotic Brownian behavior. The same conclusion was drawn from the DPD simulation data of Ref. 27, and attributed to the lack of clear time scale separation in coarse-grained simulation methods. The same conclusion applies to our MSD data presented here. Contrary to the short-time diffusion, the asymptotic Brownian behavior is clearly exhibited in the MSD data, and the values of $D_T(\phi_c)$ thus obtained are reported in Table II.

Next, Fig. 6 shows data for the time-dependent quantity $D_T(t)$ from Eq. (31) using $n = 12$ in the inverse power-law potential (the same kind of behavior is obtained for $n = 48$). For each volume fraction, $D_T(t)$ reaches a plateau at long times, which defines the asymptotic tracer diffusion coefficient $D_T(\phi_c)$. The values thus obtained are also reported in Table II. It is interesting to note that as the volume fraction increases, the curve $D_T(t)$ exhibits a peak at short times. As noted above, the MSD data cannot be used to define a short-time diffusion coefficient D_T^S for the present simulations. However, using the short-time maximum in $D_T(t)$ we can define an effective transport coefficient $\tilde{D}_T^S$, which we will below compare with the actual values of D_T^S as obtained from more microscopic simulations or experiments. The values of $\tilde{D}_T^S(\phi_c)$ are also displayed in Table II.

To further clarify the role of the HIs in the SRD-MD simulations, we have carried out additional Brownian dynamics (BD) simulations with the same colloid size and colloid-colloid IP potential (given by Eq. (8), with $n = 12$). In these simulations, the Langevin equation, in which the inertia term is neglected, has been solved for each colloid, with a time step $\Delta t_{BD} = 5 \times 10^{-7}$ s (see Ref. 38 for more details concerning the BD algorithm). Figure 7 shows the log-log plot of the MSD data. As expected, the ballistic regime is virtually absent for the current choice of parameters for the SRD-MD method. Overall, the behavior of the MSDs for BD simulations is very similar to those of SRD-MD, confirming the conclusion that the time scale separation is not present in SRD-MD data. The values of $D_T(\phi_c)$ from BD are also reported in Table II.

TABLE II. Values of the asymptotic tracer diffusion coefficient D_T obtained from both MSD and $D_T(t)$ (time integral of the v.a.c.f.) in SRD-MD simulations; values of the effective short-time transport coefficient $\tilde{D}_T^S$ in SRD-MD simulations (no value of $\tilde{D}_T^S$ is given for $\phi_c = 0.001$, because this is the case with only one colloid and there is no peak at short time in the $D_T(t)$ curve); and values of D_T in BD simulations (for $\phi_c = 0.001$, only one colloid is present and the given value corresponds to $D_0 = k_B T/6\pi\eta a_c$). The values are given as a function of the colloidal volume fraction and expressed in units of 10^{-13} m^2 s^{-1}. For all these values, the colloid-colloid interaction potential corresponds to Eq. (8), with $n = 12$.

ϕ_c	0.001	0.1	0.2	0.3	0.4	0.5	0.6
D_T [a]	7.2 ± 0.3	5.66 ± 0.07	4.38 ± 0.04	3.04 ± 0.07	1.74 ± 0.05	0.73 ± 0.04	0.11 ± 0.03
D_T [b]	7.2 ± 0.2	5.66 ± 0.07	4.39 ± 0.05	3.05 ± 0.08	1.74 ± 0.06	0.74 ± 0.04	0.11 ± 0.03
$\tilde{D}_T^S$ [c]	...	5.84 ± 0.03	4.57 ± 0.02	3.53 ± 0.01	2.732 ± 0.003	2.125 ± 0.005	1.66 ± 0.01
D_T [d]	7.15	5.59 ± 0.26	4.09 ± 0.04	2.81 ± 0.05	1.58 ± 0.07	0.61 ± 0.01	0.06 ± 0.01

[a]From MSD in SRD-MD.
[b]From $D_T(t)$ in SRD-MD.
[c]From $D_T(t)$ in SRD-MD.
[d]From MSD in BD.

Finally, in Fig. 8 we summarize our data for the scaled diffusion coefficients $D_T(\phi_c)/D_0$ as obtained from the SRD-MD and BD simulations. For comparison, we also show the scaled effective short time transport coefficients $\tilde{D}_T^S(\phi_c)/D_0$ from the SRD-MD simulations. As can be seen in this figure, the SRD-MD scaled diffusion coefficients $D_T(\phi_c)/D_0$ are very close but slightly larger than those from the BD simulations. This is in accordance with 2D results in Ref. 17 and the idea that momentum propagation enhances tracer diffusion.

D. Comparison with other results

To compare our results with those in the literature, we need to rescale the colloid volume fraction appropriately (see for example Refs. 27, 36, and 39). In order to compare with hard sphere colloids, the core volume fraction is converted to an effective volume fraction so that the observed beginning of crystallization corresponds to the freezing transition, which is known to occur at a volume fraction of 0.494 for a hard sphere fluid (see Refs. 36 and 39 for details). However, it is a nontrivial task to pinpoint the precise value of the bare volume fraction ϕ_c where crystallization commences. In our system we start to observe organized structures of colloids for some simulations at $\phi_c \approx 0.57$ for $n = 12$. Khrapak *et al.* have reported freezing data obtained by simulations for inverse-power potentials.[40] But here, in order to determine more precisely the volume fraction that corresponds to the beginning of crystallization in our simulations, we preferred to use the criterion proposed by Löwen *et al.*,[41] which states that the ratio of the long-time to short-time self-diffusion coefficients has a universal value of 0.1 along the fluid freezing line. This criterion has been confirmed by experimental data and it appeared to work well also for our simulation data. Assuming that we can identify $\tilde{D}_T^S \approx D_T^S$ (see below), the freezing transition in our simulations occurs at $\phi_c = 0.58$ for $n = 12$ and at $\phi_c = 0.52$ for $n = 48$ (see Fig. 8). As a consequence,

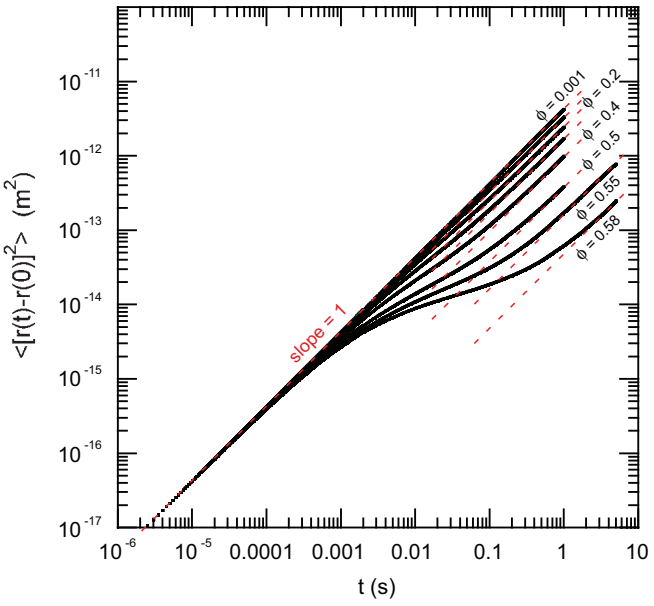

FIG. 7. Log-log plot of the colloid mean-square displacement in BD simulations, for colloid volume fractions of 0.001, 0.1, 0.2, 0.3, 0.4, 0.5, 0.55, and 0.58. The power of the IP colloid-colloid potential is $n = 12$.

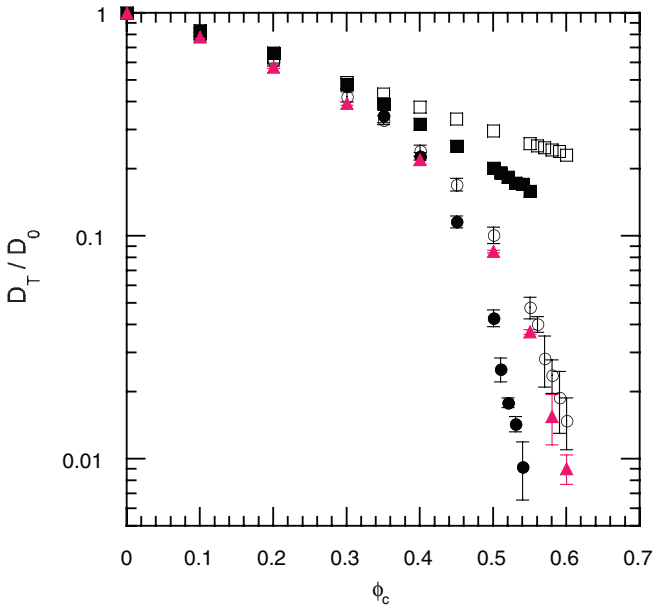

FIG. 8. Scaled effective short-time (squares) and asymptotic (circles) tracer diffusion coefficients as a function of the colloid volume fraction, for the exponents of the IP colloid-colloid interaction potential $n = 12$ (open symbols) and $n = 48$ (closed symbols). When not shown, error bars are smaller than the size of the symbols. The asymptotic tracer diffusion coefficient as obtained from the BD simulations is also shown (triangles), in the case $n = 12$.

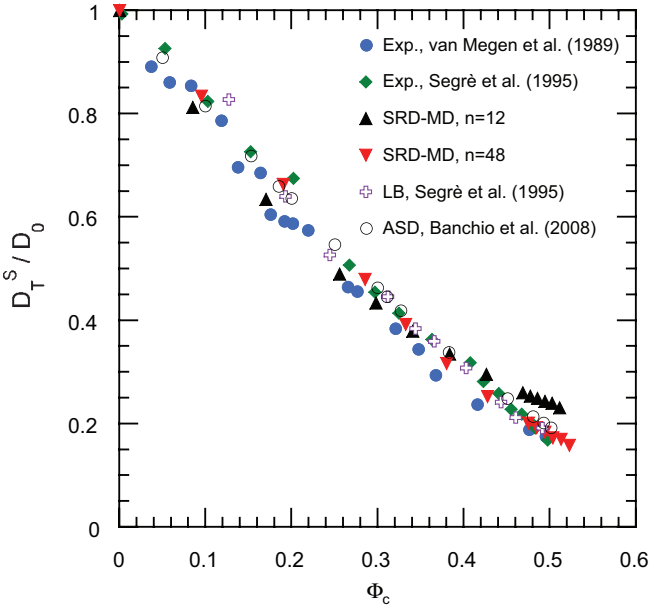

FIG. 9. Comparison of the effective quantity $\tilde{D}_T^S/D_0$ from SRD-MD results with the short-time diffusion coefficients as determined from experimental results[36,39] and other simulation results based on the Lattice-Boltzmann (LB) (Ref. 36) and accelerated Stokesian dynamics (ASD).[42] Φ_c denotes the rescaled colloid volume fraction (see text for details).

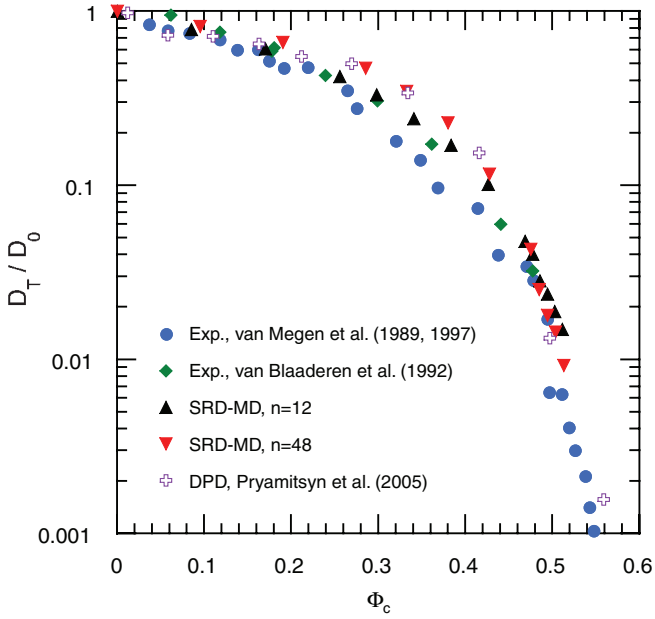

FIG. 10. Asymptotic diffusion coefficient: comparison of our simulation results with experimental results from Refs. 35, 39, and 43 and with other simulation results using dissipative particle dynamics (DPD).[27] Φ_c denotes the rescaled colloid volume fraction (see text for details).

in the following, we will use the rescaled volume fractions $\Phi_c = \frac{0.494}{0.58}\phi_c$ for $n = 12$, and $\Phi_c = \frac{0.494}{0.52}\phi_c$ for $n = 48$.

Considering first the issue of the short-time diffusion coefficient, Fig. 9 shows the comparison between our effective values $\tilde{D}_T^S(\Phi_c)/D_0$, experimental results,[36,39] and simulation results from Lattice-Boltzmann[36] and accelerated Stokesian dynamics[42] techniques. In all these other cases, a well-defined value of the short time diffusion coefficient D_T^S was determined. Our effective $\tilde{D}_T^S$ (especially for the case $n = 48$) turn out to be in good agreement with all the other results, despite the fact that using the MSD it was not possible to determine any short time diffusive behavior. This agreement indicates that some features of the expected microscopic behavior at short times are present in the SRD-MD simulations despite the coarse-grained nature of the solvent.

In Fig. 10, we compare our data for the true (long time) diffusion coefficients with those obtained from experimental results,[35,39,43] and other simulation results from the DPD (Ref. 27) technique. The difference observed in our simulations between $n = 12$ and $n = 48$ after the rescaling of the volume fraction shows that the long-time diffusion coefficient is affected by the colloid-colloid interaction potential. Quite a good agreement is obtained in between our simulation results (especially with $n = 12$) and experimental data. Except for the highest volume fractions, our SRD-MD simulation results fit the experimental data better than the DPD simulation results from Pryamitsyn *et al.*,[27] where hydrodynamic interactions are included and where a 6-12 Lennard-Jones potential is used for the colloid-colloid interaction. It is worth noting that, in their study, they also rescale the colloid volume fraction but using a different criterion. They estimated from their simulation results that the large-scale particle diffusion is arrested at 0.68, while it is known to occur at the glass transition volume fraction of 0.58 in a hard sphere fluid, so that in their case $\Phi_c = \frac{0.58}{0.68}\phi_c$. This rescaling is essentially the same as the one we used for $n = 12$. In their study, the colloid-colloid interaction is treated by a 6-12 Lennard-Jones potential. According to the shape of this potential, which is in between the IP potential with $n = 12$ and the one with $n = 48$ (see Fig. 1), it seems that the rescaling they used slightly overestimates the correction applied to the data.

IV. CONCLUSIONS

In this work, we have studied the colloid tracer diffusion coefficients in a realistic model of a colloidal suspension by means of SRD-MD simulations. This technique has been chosen because of its efficiency to solve the hydrodynamics of colloids embedded in a liquid and subject to thermal fluctuations. SRD and MD have been used to simulate the dynamics of the solvent and of the colloids, respectively. These two parts are coupled by the introduction of a colloid-fluid interaction potential that intervenes in the MD steps. Special attention has been paid in the choice of the SRD parameters and of the various scales in order to keep a balance between good resolution and computational cost. The linear size of collision cells has been chosen to be equal to half the colloid radius and the mean free path of the fluid particles to one tenth of this size. As a consequence, the grid shifting procedure has been used in order to preserve Galilean invariance. The time scale has been adjusted so that the simulation correctly reproduces the colloid diffusion time. The colloid-fluid interaction potential has been tuned such that the fluid particles can penetrate in between two colloids in order to avoid spurious depletion attraction between the colloids.

The results show that the SRD-MD technique employed here is capable of properly including the essential features of the hydrodynamic interactions in a colloidal suspension. The computation of the colloid tracer diffusion coefficient under high dilution for different system sizes exhibits long-range hydrodynamic effects in agreement with theoretical predictions. The colloidal diffusive behavior as a function of the colloidal volume fraction shows the influence of both steric and HIs, and well-defined asymptotic diffusion coefficients arise, which are in good agreement with experiments and other simulation results with proper rescaling of the colloid volume fraction. However, our SRD-MD data for the MSD of the colloids cannot be used to determine a short time diffusion coefficient in agreement with the DPD simulation data of Ref. 27. Interestingly enough we can still use the short-time maximum in $D_T(t)$ to define an effective short time transport coefficient, which is in good agreement with the actual values obtained for $D_T^S(\Phi_c)/D_0$ over a range of volume fractions. This indicates that although there is no clear time scale separation in the coarse-grained SRD-MD method, some influence of the HIs to the short time dynamics of colloidal particles remains. These results are promising for the simulation of colloidal suspensions by SRD-MD. In the future, we will use this technique to study phenomena related to aggregation processes in colloidal suspensions.

ACKNOWLEDGMENTS

We acknowledge a funding from the French National Research Agency (ANR) under the Young Researchers project no. ANR-09-JCJC-0086, HYSISCO. This work has been supported in part by the Academy of Finland, in particular through its COMP CoE grant. Further support from the ERC Advanced Grant project (CROWDED-PRO-LIPIDS) is also acknowledged (I.V.). We thank Riccardo Ferrando and Santtu Ollila for fruitful discussions.

[1] D. L. Ermak, J. Chem. Phys. **62**, 4189 (1975).
[2] M. Cerbelaud, A. Videcoq, P. Abélard, C. Pagnoux, F. Rossignol, and R. Ferrando, Langmuir **24**, 3001–3008 (2008).
[3] M. Cerbelaud, A. Videcoq, P. Abélard, C. Pagnoux, F. Rossignol, and R. Ferrando, Soft Matter **6**, 370–382 (2010).
[4] M. A. Piechowiak, A. Videcoq, F. Rossignol, C. Pagnoux, C. Carrion, M. Cerbelaud, and R. Ferrando, Langmuir **26**, 12540–12547 (2010).
[5] M. A. Piechowiak, A. Videcoq, R. Ferrando, D. Bochicchio, C. Pagnoux, and F. Rossignol, Phys. Chem. Chem. Phys. **14**, 1431–1439 (2012).
[6] J. F. Brady and G. Bossis, Annu. Rev. Fluid Mech. **20**, 111 (1988).
[7] A. J. C. Ladd, J. Fluid Mech. **271**, 285 (1994).
[8] A. J. C. Ladd, J. Fluid Mech. **271**, 311 (1994).
[9] P. Ahlrichs and B. Dünweg, Int. J. Mod. Phys. C **9**, 1429 (1998).
[10] P. Ahlrichs and B. Dünweg, J. Chem. Phys. **111**, 8225 (1999).
[11] S. Ollila, C. Denniston, M. Karttunen, and T. Ala-Nissila, J. Chem. Phys. **134**, 064902 (2011).
[12] P. J. Hoogerbrugge and J. M. V. A. Koelman, Europhys. Lett. **19**, 155 (1992).
[13] P. Español and P. B. Warren, Europhys. Lett. **30**, 191 (1995).
[14] A. Malevanets and R. Kapral, J. Chem. Phys. **110**, 8605 (1999).
[15] A. Malevanets and R. Kapral, J. Chem. Phys. **112**, 7260 (2000).
[16] J. T. Padding and A. A. Louis, Phys. Rev. E **74**, 031402 (2006).
[17] E. Falck, J. M. Lahtinen, I. Vattulainen, and T. Ala-Nissila, Eur. Phys. J. E **13**, 267–275 (2004).
[18] J. T. Padding and A. A. Louis, Phys. Rev. Lett. **93**, 220601 (2004).
[19] M. Hecht, J. Harting, T. Ihle, and H. J. Herrmann, Phys. Rev. E **72**, 011408 (2005).
[20] G. Gompper, T. Ihle, D. M. Kroll, and R. G. Winkler, Adv. Polym. Sci. **221**, 1–87 (2009).
[21] A. Wysocki, C. P. Royall, R. G. Winkler, G. Gompper, H. Tanaka, A. van Blaaderen, and H. Löwen, Soft Matter **5**, 1340–1344 (2009).
[22] A. J. Banchio and G. Nägele, J. Chem. Phys. **113**, 3381–3396 (2000).
[23] E. Tüzel, M. Strauss, T. Ihle, and D. M. Kroll, Phys. Rev. E **68**, 036701 (2003).
[24] N. Kikuchi, C. M. Pooley, J. F. Ryder, and J. M. Yeomans, J. Chem. Phys. **119**, 6388 (2003).
[25] T. Ihle and D. M. Kroll, Phys. Rev. E **63**, 020201 (2001).
[26] H. Löwen, Phys. Rev. E **53**, R29 (1996).
[27] V. Pryamitsyn and V. Ganesan, J. Chem. Phys. **122**, 104906 (2005).
[28] J. Lyklema, *Fundamentals of Interface and Colloid Science, Vol. 1: Fundamentals* (Academic, London, 1991).
[29] L. Bergström, Adv. Colloid Interface Sci. **70**, 125–169 (1997).
[30] M. Hütter, J. Colloid Interface Sci. **231**, 337–350 (2000).
[31] R. Hogg, T. Healy, and D. Fuerstenau, Trans. Faraday Soc. **62**, 1638–1651 (1966).
[32] T. Ihle, E. Tüzel, and D. M. Kroll, Phys. Rev. E **70**, 035701 (2004).
[33] S. C. Ying, I. Vattulainen, J. Merikoski, T. Hjelt, and T. Ala-Nissila, Phys. Rev. B **58**, 2170–2178 (1998).
[34] A. van Veluwen and H. N. W. Lekkerkerker, Phys. Rev. A **38**, 3758 (1988).
[35] W. van Megen, S. M. Underwood, J. Müller, T. C. Mortensen, S. Henderson, J. L. Harland, and P. Francis, Prog. Theor. Phys. Suppl. **126**, 171 (1997).
[36] P. N. Segrè, O. P. Behrend, and P. N. Pusey, Phys. Rev. E **52**, 5070 (1995).
[37] M. Medina-Noyola, Phys. Rev. Lett. **60**, 2705 (1988).
[38] A. Videcoq, M. Han, P. Abélard, C. Pagnoux, F. Rossignol, and R. Ferrando, Physica A **374**, 507–516 (2007).
[39] W. van Megen and S. M. Underwood, J. Chem. Phys. **91**, 552 (1989).
[40] S. A. Khrapak and G. E. Morfill, Phys. Rev. Lett. **103**, 255003 (2009).
[41] H. Löwen, T. Palberg, and R. Simon, Phys. Rev. Lett. **70**, 1557 (1993).
[42] A. J. Banchio and G. Nägele, J. Chem. Phys. **128**, 104903 (2008).
[43] A. van Blaaderen, J. Peetermans, G. Maret, and J. K. G. Dhont, J. Chem. Phys. **96**, 4591 (1992).